

Direct measurement of cantilever spring constants and correction for cantilever irregularities using an instrumented indenter

Z. Charles Ying^{a)}

National Institute of Standards and Technology, Gaithersburg, Maryland 20899
and NanoLane, LLC, Boyds, Maryland 20841

Mark G. Reitsma and Richard S. Gates

National Institute of Standards and Technology, Gaithersburg, Maryland 20899

(Received 22 August 2006; accepted 14 May 2007; published online 25 June 2007)

A method is presented that allows direct measurement of a wide range of spring constants of cantilevers using an indentation instrument with an integrated optical microscope. An uncertainty of less than 10% can be achieved for spring constants from 0.1 to 10^2 N/m. The technique makes it possible to measure the spring constant at any desired location on a cantilever of any shape, particularly at the tip location of an atomic force microscopy cantilever. The article also demonstrates a technique to detect and correct apparent length anomalies of cantilevers by analyzing spring constants at multiple positions. © 2007 American Institute of Physics.

[DOI: [10.1063/1.2747095](https://doi.org/10.1063/1.2747095)]

I. INTRODUCTION

Atomic force microscopy (AFM) is widely used for imaging surfaces,¹⁻³ for manipulating nanoparticles and fabricating nanostructures,⁴ and for measuring nanomechanical properties,^{5,6} including adhesion and friction forces,⁷⁻¹¹ with nanonewton or piconewton sensitivity and nanometer or higher spatial resolution. The central component of an atomic force microscope is a flexible cantilever with a tip. Quantitative force measurements using the AFM technique require knowledge of the cantilever spring constant or stiffness at the tip location.¹²⁻¹⁵ Uncertainties in spring constant values are recognized as a major source of errors in quantitative force measurements.^{2,3,12-15} Accurate spring constant calibration is also important to other cantilever-based technologies such as mass-sensitive detection of chemical and biological materials¹⁶ and certain components (e.g., accelerometers) of microelectromechanical systems (MEMSs).¹⁷ Due to lack of precise control of cantilever dimensions during commercial manufacturing, large spring constant ranges, often a factor of 2 or more, are commonly found in commercial cantilever specifications provided by the manufacturers. As a result, individual cantilevers need to be calibrated by the user in order to achieve quantitative AFM measurements.

Several experimental techniques have been developed to measure spring constants of AFM cantilevers, particularly the spring constant due to the cantilever deflection in the normal or z direction (see Fig. 1). In the added mass method developed by Cleveland *et al.* (Cleveland method), a spring constant is extracted from an analysis of the change in the resonant frequency of a cantilever when microspheres of known mass values are attached near the free end of the

cantilever.^{12,18} The unloaded resonance technique developed by Sader *et al.* (Sader method) relates the spring constant to the resonant frequency, quality factor, and plan view dimensions of a cantilever.¹⁹ The spring constant of a cantilever can also be obtained by analyzing its thermal noise spectrum, provided that the thermal noise signal at the fundamental frequency of harmonic oscillations is used.²⁰⁻²² In the static and dynamic Euler-Bernoulli methods,²³ the spring constant is calculated from modulus and resonant frequency, respectively, in addition to the cantilever dimensions and material density. The above calibration methods relate the spring constant value to other measurable quantities such as frequency, mass, and cantilever dimensions. The spring constant can also be measured using a reference calibration method by pressing the cantilever to be calibrated against a reference cantilever²⁴⁻²⁸ or another object of known stiffness.²⁹⁻³¹

After calibration using one or more of the methods described above, spring constant uncertainties are reported in a range between 5% and 30%.^{12-15,30} The remaining uncertainties are commonly attributed to deviations of cantilever geometry from an ideal shape, presence of surface coating materials on a cantilever, and issues specific to individual calibration methods. Accuracy of the Cleveland method, for example, depends to a large extent on the ability to precisely determine the microsphere mass. The Sader method was developed for beam shaped cantilevers of rectangular cross section. Many beam shaped cantilevers that are made of single crystal silicon often have trapezoidal cross sections, and appropriate corrections³² should be made in order to accurately measure the spring constant using the Sader method for a cantilever of large thickness.

It should also be pointed out that a calibrated spring constant value often refers to the whole cantilever, i.e., the spring constant at the free end of the cantilever. However, AFM measurements often use an integrated tip on the cantilever and the tip is usually not located exactly at the free end,

^{a)} Author to whom correspondence should be addressed; Present address: Division of Materials Research, National Science Foundation, Arlington, Virginia 22230; electronic mail: cying@nsf.gov

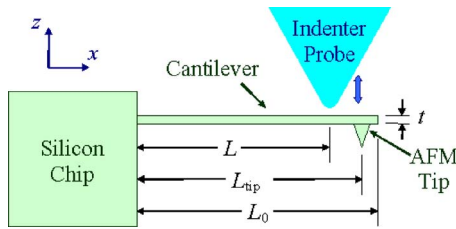


FIG. 1. (Color online) Schematic diagram of an AFM cantilever of length L_0 and thickness t . An indenter probe can be positioned at any location L of the cantilever to measure the spring constant at that location.

but some distance away. Consequently, the spring constant at the tip location is different from that at the free end. While this problem can be remedied by an off-end correction,¹² a more desirable approach is to have a technique capable of measuring the spring constant directly at the tip location, thus eliminating the uncertainty associated with the off-end correction step.

In this article, we report direct measurements of spring constants at desired locations on AFM cantilevers using an instrumented indentation apparatus. Because of the low loads used in these experiments, the indenter probe actually does not indent the cantilever material. Rather the apparatus measures force versus distance as the cantilever deflects. The spring constant is obtained from the slope of the force-distance data. The approach is similar to that reported previously³³ with two important improvements:

- The lower limit of the spring constant range that can be measured using the instrumented indenter method has been extended by an order of magnitude from 1 to 0.1 N/m. This improvement allows contact-mode cantilevers, in addition to tapping-mode and force modulation cantilevers, to be calibrated.
- We have used an instrumented indenter with an integrated optical microscope and a calibrated distance between an indenter probe and optical microscope so that spring constant measurements can be performed at any location on a cantilever with micrometer positioning accuracy. This capability is particularly useful in measuring the spring constant at the AFM tip location.

The article will also show that some cantilever irregularities can be detected by a careful study of spring constants obtained at multiple locations on a cantilever. As an example, cantilevers missing some parts of the SiO_2 supporting layer between the cantilevers and silicon chip are examined. The missing SiO_2 layer, which is difficult to observe using optical microscopy, could lead to incorrect spring constant values if undetected.

II. DESCRIPTION OF INSTRUMENTS

The experiments were carried out using an instrumented indenter based on a three-plate capacitive transducer.³⁴ (Hysitron, TriboIndenter) and an atomic force microscope (Veeco Metrology, MultiMode, NanoScope IIIa). Both instruments were supported on structures with vibration isolation systems.

A cone shaped, diamond indenter probe with a spherical apex of $0.5 \mu\text{m}$ radius was used to measure cantilever spring constants (see Fig. 1). The indenter apparatus and cantilevers were placed in a nitrogen environment at a temperature of $22.0 \pm 0.1^\circ \text{C}$ and relative humidity of $< 1\%$. It was found in our experiments that, by placing the TriboIndenter in the low humidity environment, its transducer produced much less random variations, especially at low frequencies. High-frequency noises, originated mainly from the transducer controller electronics, can be reduced by filtering and data averaging. It should also be noted that the TriboIndenter operation parameters, including the electrostatic force constant, plate spacing, and sensor bias of the high-voltage power supply, must be carefully calibrated so that an “indent” performed in air produced zero net force at all displacement values. All these are crucial to achieve accurate measurements of spring constants, especially those below 1 N/m.

The AFM was used for cantilever spring constant measurements using the Cleveland and Sader methods. Gold microspheres (Alfa Aesar) were used as added masses in experiments using the Cleveland method. The AFM experiments were performed in air at a temperature of $21.0 \pm 0.1^\circ \text{C}$ and humidity of $45\% \pm 5\%$.

A. Indenter probe positioning accuracy

The indentation apparatus used in this study had a built-in optical microscope with a video camera. Cantilevers were mounted on top of precision linear stages with location decoding every $0.5 \mu\text{m}$, which provided controlled translation in the x and y directions. The combination of the optical microscope system and the precision linear stages allowed imaging of cantilevers, accurate measurement (within $2 \mu\text{m}$) of plan view dimensions of cantilevers, and accurate positioning (within $2 \mu\text{m}$) of the indenter probe at a desired location.

In order to achieve accurate indenter probe positioning, the distance between the apex of an indenter probe and the center of the microscope field of view (FOV) was calibrated. The distance calibration was then verified using a two-step process: First, the x - y linear stages moved an aluminum sample to the coordinates at the center of an “H” pattern formed by seven indentations in the initial distance calibration. An examination was made to ensure that the center indent of the “H” pattern remained at the center of the microscope FOV. Second, an additional indentation was performed and its location was examined. This two-step process was performed before and after spring constant measurements, and repeated every a few hours in long experiments, to ensure that uncertainties of indenter probe positioning were kept within $2 \mu\text{m}$.

B. Cantilevers

Three AFM cantilever systems, all made of silicon, were used in this study: one developed at the National Institute of Standards and Technology (NIST) and the other two commercially available.

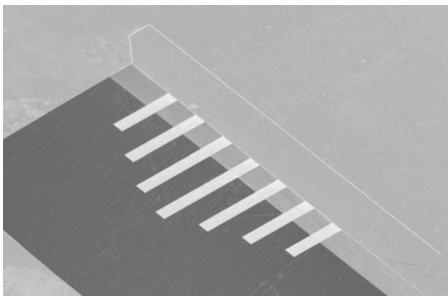


FIG. 2. A SEM image of a seven-beam experimental cantilever array developed at NIST.

A scanning electron microscopy (SEM) image of a seven-beam experimental cantilever array developed at NIST is shown in Fig. 2. The lengths of the seven tipless cantilevers vary from 300 to 600 μm in increments of 50 μm , with uncertainties of less than 1 μm . The cantilever widths are all 50 μm . Manufactured from a silicon-on-insulator wafer, the cantilevers have well controlled thickness of $1.39 \pm 0.01 \mu\text{m}$.

Figure 3 shows a commercial cantilever commonly used for force modulation and noncontact measurements (Veeco Probe, FESP). The free end of the cantilever has a triangular shape, instead of a square end as in an ideal beam shaped cantilever. This cantilever is $240 \pm 2 \mu\text{m}$ long, measured from the cantilever base to the triangular end. The cross section of the cantilever is a trapezoid, which is common for commercial AFM cantilevers made of single crystal silicon. The major and minor widths of the trapezoid for the main part of the cantilever are measured to be 30 ± 2 and $19 \pm 2 \mu\text{m}$, respectively. The typical thickness value of this type of cantilevers, 3 μm , is provided by the manufacturer.

The third cantilever system used in this study is a commercial three-beam cantilever array (Veeco Probe, CLCF). Its plan view geometry is shown in Fig. 4. The lengths of long, medium, and short cantilevers, measured from the silicon chip edge, are 425 ± 2 , 226 ± 2 , and $124 \pm 2 \mu\text{m}$, respectively. The cross section of these cantilevers, manufactured using a special procedure, is rectangle. The measured cantilever width is $29 \pm 2 \mu\text{m}$. The typical thickness value of this type of cantilevers, 2 μm , is provided by the manufacturer.

All three cantilever systems had beam shaped cantilevers. For a beam shaped cantilever, the spring constant k at location L , measured from the anchored end (usually the silicon chip edge, see Fig. 1), is given by^{15,35}

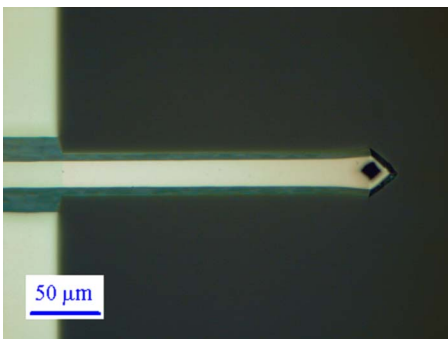


FIG. 3. (Color online) An optical image (plan view) of a commercial cantilever commonly used for force modulation.



FIG. 4. (Color online) An optical image (plan view) of a three-beam cantilever array.

$$k = \frac{3E^*I}{L^3}, \quad (1)$$

where E^* is the appropriate plane-strain elastic modulus of the cantilever material and I is the ratio of the moment of inertia to the mass of the beam. For an anisotropic material, e.g., single crystal Si, the appropriate elastic modulus is a function of direction so care must be taken in its determination.^{35,36} In the special case of a rectangular cross section, Eq. (1) becomes

$$k = \frac{E^*wt^3}{4L^3}, \quad (2)$$

where w is the cantilever width and t its thickness. There is an inverse cubic relationship between the spring constant k and distance L .

III. RESULTS AND DISCUSSION

Three sets of typical force-distance data measured using the indentation apparatus are presented in Fig. 5. A preload was used by the indentation apparatus to establish the contact point between the indenter probe and cantilevers. This contact point defines the zero distance in Fig. 5. The instrument manufacturer has set the preload at 2 μN , which is appropriate for indentation experiments. During the spring constant measurements, the preload was reduced to 0.5 μN . This change decreased cantilever deflection due to the preload.

Each set of the data in Fig. 5 follows a straight line as expected from Hooke's law, $F=kz$. Their slopes, or the spring constant values, are $21.20 \pm 0.07 \text{ N/m}$ (0.3%), $2.148 \pm 0.004 \text{ N/m}$ (0.2%), and $0.191 \pm 0.006 \text{ N/m}$ (3.1%).³⁷

The forces on the cantilevers were kept below 10 μN in the experiments, as shown in Fig. 5. Maximum displacements from 10 nm to 1 μm were used, depending on the spring constant. A more compliant spring requires a larger

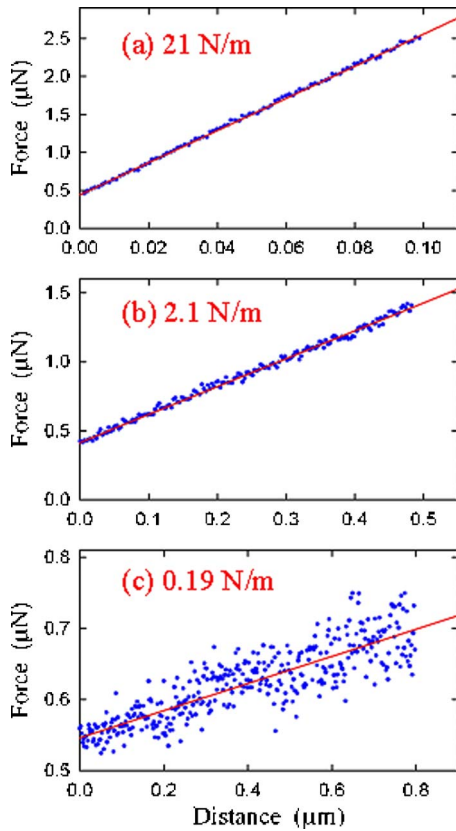


FIG. 5. (Color online) Examples of force-distance data measured using the indentation instrument (dots) and their linear fits (solid lines).

value of maximum displacement to provide adequate change in force as the force noise floor was the limiting factor.

A. Accuracy

To test the accuracy of spring constant measurements using the indentation apparatus, especially for spring constants of less than 1 N/m, we compare spring constant values obtained using several methods. The comparison is made on the seven-beam experimental cantilever array developed at NIST shown in Fig. 2.

Spring constants were measured using the indenter on the six cantilevers longer than $300\ \mu\text{m}$ at a common distance of $300 \pm 2\ \mu\text{m}$ from the silicon chip edge. The average value of six measurements is $k = 0.219 \pm 0.010\ \text{N/m}$. As shown in Table I, this value agrees well with the spring constant values measured using three other techniques: a NIST-developed, SI-traceable electrostatic force balance (EFB),³⁸ dynamic Euler-Bernoulli method,²³ and the Sader method.¹⁹ The same seven-beam cantilever array was used in the experiments using the instrumented indenter, dynamic Euler-Bernoulli, and

TABLE I. Spring constant values of the NIST cantilever array at $300\ \mu\text{m}$ from the silicon chip edge, measured using four techniques.

Technique	Spring constant (N/m)
Electrostatic force balance (from Ref. 36)	0.210 ± 0.006
Dynamic Euler-Bernoulli method	0.209 ± 0.005
Resonance (Sader) method	0.216 ± 0.012
Instrumented indenter method	0.219 ± 0.010

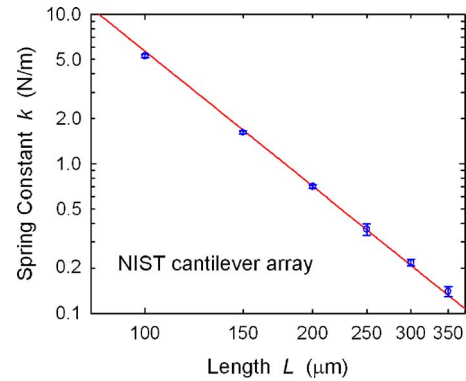


FIG. 6. (Color online) Spring constant (circles) measured at different locations of a cantilever array developed at NIST shown in Fig. 2. The solid line, drawn without any adjustable parameter, is the expected dependence of spring constant on cantilever length, Eq. (1).

Sader methods. A different seven-beam cantilever array from the same fabrication batch was used in the EFB experiment. Possible spring constant differences among the cantilever arrays, fabricated in a same batch, should be no more than 3% based on resonance measurements, therefore an uncertainty of $\pm 0.006\ \text{N/m}$ was assigned.³⁶ The spring constant value obtained using the Euler-Bernoulli method²³ is computed from the measured resonant frequency and cantilever dimensions. This approach avoids potential errors introduced by calculating spring constant using Eq. (2) through the use of an incorrect modulus value.

Figure 6 shows spring constant values (circles) measured using the instrumented indenter method at different distances L on the experimental cantilever array. The solid line represents the Euler-Bernoulli relationship [Eq. (1)] pinned at the SI-traceable EFB spring constant value of $0.210 \pm 0.006\ \text{N/m}$ at $300\ \mu\text{m}$.³⁶ The spring constants measured using the instrumented indenter method agree well with the expected values, and the dependence of spring constant on distance L follows the expected inverse cubic relationship. The deviations of individual data points from the solid line are less than 8%. These results suggest that the instrumented indenter method is able to provide accurate measurements of spring constants, with uncertainties of less than 10%, both above and below 1 N/m.

The highest spring constant value that we measured was 250 N/m. It should be pointed out that the stiffness of the metal springs in the indenter transducer (208.1 N/m in our instrument) is not the upper limit of the technique. The force exerted on the indenter probe by a deflected cantilever is balanced not only by the mechanical force due to the metal springs but also by the electrostatic force generated by the transducer. By keeping thermal drift of the indenter probe in the normal direction well below 0.1 nm/s, one can extend the technique to $10^3\ \text{N/m}$. This means that a very wide range of spring constant (four orders of magnitude, from 0.1 to $10^3\ \text{N/m}$) can be measured using this technique. Approaching $10^4\ \text{N/m}$ or larger, one needs to avoid or correct for local deformation of the cantilever material around the diamond indenter probe.

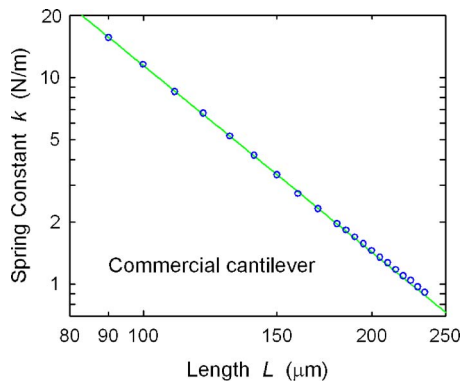


FIG. 7. (Color online) Spring constants (circles) measured at different locations of the force modulation cantilever shown in Fig. 3. The solid line is a fit to the experimental data using Eq. (1).

B. Length dependence

Next we study a cantilever with unknown spring constant. The plan view geometry of this cantilever, typically used in AFM force modulation experiments, is shown in Fig. 3. Spring constants were measured along the long axis of the cantilever at various distances from the silicon chip edge. The results are shown in Fig. 7. The solid line in the figure is a fit to the experimental data using Eq. (1) with one adjustable parameter, i.e., $3E^*I$. The experimental data follow this straight line with a slope of -3 in the double logarithmic plot. In other words, the measured spring constant values follow the expected inverse cubic dependence. The deviations of individual data points from the solid line are 4% or less.

The tip on this cantilever was measured to be at $220 \pm 2 \mu\text{m}$ from the base of the cantilever or $20 \pm 2 \mu\text{m}$ from the free end of the cantilever. The spring constant measured at this location is $1.094 \pm 0.017 \text{ N/m}$.³⁷ This value is within the manufacturer's specification (1–5 N/m).

A measurement of spring constant at the tip location is direct using the instrumented indenter method. This is in contrast to other spring constant measurement methods, which provide a spring constant value at the free end of a cantilever. Because the spring constant value required in AFM measurements is at the location of an AFM tip, an additional step is needed to compute the spring constant at the tip location from that at the free end. This computation step introduces additional uncertainties. This is particularly true for cantilevers with triangular ends.

C. Length anomaly correction

Measurement of spring constants at multiple locations can reveal geometrical irregularities in cantilevers. Here we present an example that uses the instrumented indenter method for detection and correction for cantilever length anomalies. This is performed using a three-beam cantilever array; the plan view geometry of which is shown in Fig. 4.

Figure 8(a) shows spring constants (symbols) of the three cantilevers of the three-beam array plotted versus distance measured from the silicon chip edge. In contrast to a single curve expected for the three cantilevers with identical width and thickness, three different curves are observed. At a

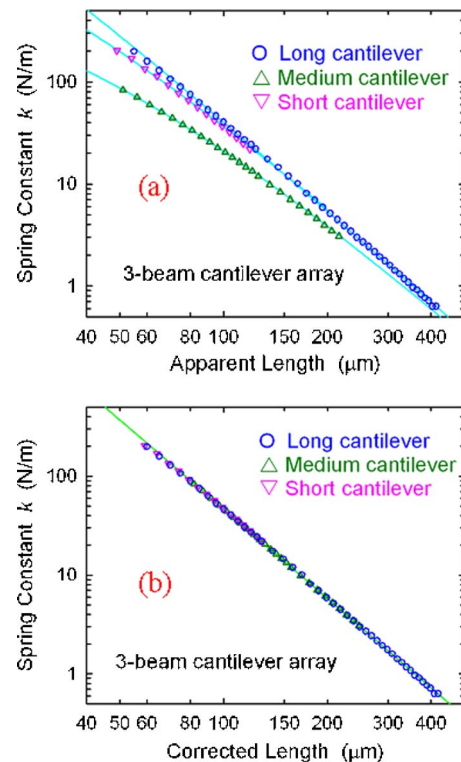


FIG. 8. (Color online) Spring constants (symbols) measured at different locations of the three-beam cantilever array shown in Fig. 4. The data are plotted using (a) the apparent cantilever lengths as measured from the edge of the silicon chip and (b) the corrected values of cantilever lengths.

given distance, the spring constant value of the short cantilever is somewhat lower than that of the long cantilever, and a much smaller spring constant value is observed for the medium cantilever. In addition, the experimental data [symbols in Fig. 8(a)] exhibit substantial deviations from the expected inverse cubic dependence. The curvature of the experimental data in the double logarithmic plot of Fig. 8(a) suggests that these cantilevers are longer than the values based on the plan view measurements.

Another indication of longer cantilevers is found by comparing spring constants determined using different techniques. As shown in Table II, the spring constant values of the cantilevers measured using the instrumented indenter and Cleveland methods are similar. These two methods are not very sensitive to errors in cantilever length. On the other hand, the spring constant value of the medium cantilever

TABLE II. Spring constant values, obtained using different techniques, of the three-beam cantilever array. The apparent cantilever lengths, measured from the silicon chip edge to the free ends of the cantilevers, are used in the spring constant calculations. (The Sader method value is not available for the short cantilever.)

Technique	Spring constant (N/m)		
	Long	Medium	Short
Instrumented indenter method	0.583 ± 0.033	2.68 ± 0.11	19.5 ± 1.0
Added mass (Cleveland) method	0.608 ± 0.052	2.59 ± 0.09	19.7 ± 1.7
Resonance (Sader) method	0.602 ± 0.008	2.39 ± 0.06	...
Static Euler-Bernoulli method	0.641 ± 0.028	3.91 ± 0.17	19.1 ± 0.8

measured using the Sader method is significantly smaller, while a substantially larger value is obtained from the static Euler-Bernoulli method. The spring constant values reported in Table II use the apparent cantilever lengths, measured from the plan view through an overhead optical microscope. The formula to compute spring constants using the Sader method has a linear dependence on the cantilever length.¹⁹ If an apparent cantilever length that is shorter than the true cantilever length is used, the Sader method will provide a lower value of spring constant. On the other hand, Eq. (1) indicates that a much larger spring constant value will be obtained from the static Euler-Bernoulli model if an apparent cantilever length shorter than the true cantilever length is used. The data presented in Table II are consistent with this analysis, supporting the idea that the cantilevers in this three-beam array, especially the medium cantilever, are significantly longer than they appear from plan view dimensions.

Let us assume that the true length L of a cantilever has two components: an apparent length l , measured from the silicon chip edge, and an additional contribution Δl . The spring constant is then given by

$$k = \frac{3E^*I}{L^3} = \frac{3E^*I}{(l + \Delta l)^3}, \quad (3)$$

Clearly, the dependence of spring constant k on apparent length l is no longer inverse cubic for a nonzero Δl . The difference between the true spring constant given in Eq. (3) and an incorrect value computed by $k' = 3E^*I/l^3$ is

$$\Delta k = k - k' = \frac{3E^*I}{(l + \Delta l)^3} - \frac{3E^*I}{l^3}, \quad (4)$$

which can be approximated by

$$\Delta k = -\frac{3\Delta l}{l} \frac{3E^*I}{L^3} = -\frac{3\Delta l}{l} k, \quad (5)$$

if $|\Delta l| \ll l$. This difference is proportional to Δl . For a fixed value of Δl , it decreases as l increases.

The experimental data [symbols in Fig. 8(a)] are fitted to Eq. (3) [lines in Fig. 8(a)] with two adjustable parameters: $3E^*I$ and Δl . The additional lengths for the long, medium, and short cantilevers, determined from the fittings, are $\Delta l = 5 \pm 3$, 31 ± 3 , and $10 \pm 3 \mu\text{m}$, respectively. Note that a much greater value of additional length is seen for the medium cantilever than the other two cantilevers.

The spring constants measured using the instrumented indenter method are plotted versus corrected length, $L = \Delta l + l$, in Fig. 8(b). Now all three sets of data superimpose and follow a single line. The inverse cubic dependence between the spring constant and length is restored.

To find the origin of the additional cantilever lengths in this three-beam array, we performed SEM measurements of the cantilevers. As shown in Fig. 9, all three cantilevers are not supported at the silicon chip edge. The SiO_2 supporting layer between the silicon cantilevers and the silicon chip was etched away, resulting in undercut for all three cantilevers. The undercut values, determined from the SEM images, are 2 ± 1 , 25 ± 5 , and $3 \pm 1 \mu\text{m}$ for the long, medium, and short cantilevers, respectively. The undercut is smallest for the

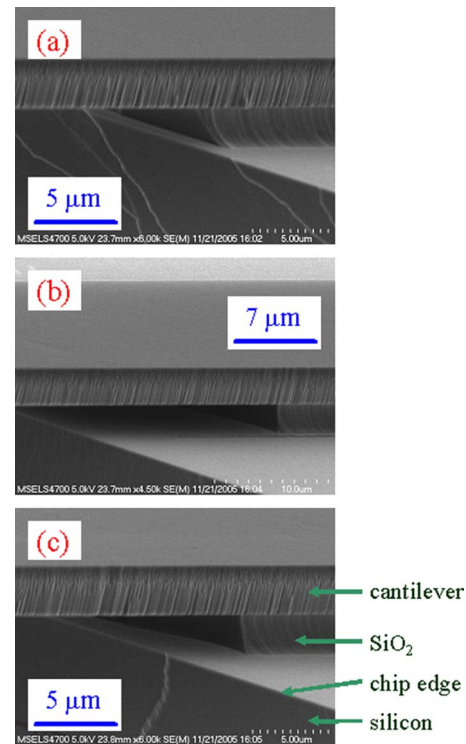


FIG. 9. (Color online) SEM images of the three-beam cantilever array near the base regions of (a) the long, (b) medium, and (c) short cantilevers.

long cantilever and largest for the medium cantilever. This trend is in agreement with the results obtained from the spring constant measurements.

It is noted, however, that the Δl values obtained from the instrumented indenter method are close to but consistently greater than the undercut values measured by SEM. A possible explanation for this difference is that a cantilever is not anchored perfectly at the location where the cantilever contacts the SiO_2 supporting layer underneath. Equations (1) and (2) are derived under the boundary conditions that both the cantilever deflection and its derivative relative to the chip are zero at $L=0$. In reality, cantilevers are not perfectly clamped and have a small, but nonzero deflection at the contact point of the cantilever to the supporting materials.³⁹ In other words, the effective length of a cantilever should be a little longer than the distance measured from the contact point. The presence of the supporting layer made of SiO_2 , which has its modulus lower than that of Si, may result in additional weakening of the cantilever anchoring.

The examples presented above illustrate the ability of a position dependence study of spring constant to detect and correct for cantilever length anomalies. Other cantilever irregularities, such as nonuniform cantilever thickness or width, could also be detected. Accurate determination of the location at which spring constant is measured is the key. This was achieved in our experiments using an instrumented indenter with built-in precision linear stages and through accurate positioning calibration performed before and after spring constant measurements. Similar experiments could be performed using an AFM instrument employing the reference calibration method, provided that probe could be positioned with micrometer or better accuracy.

IV. SUMMARY

An instrumented indenter, with an integrated optical microscope and precision linear stages, was used to measure spring constants of AFM cantilevers with micrometer positioning accuracy. The data suggest that the instrumented indenter method is capable of measuring spring constants over the range from 0.1 to 200 N/m with an uncertainty of less than 10%. This wide spring constant range covers AFM cantilevers used in all major modes, including tapping mode, noncontact mode, force modulation mode, contact mode, and force measurements of nonbiological materials.

A chief advantage of the instrumented indenter method is its ability to measure spring constants of cantilevers of any shape and at any location, especially at the position of an AFM tip. It eliminates the need to compute the spring constant at the tip position from that at the cantilever's free end, as required using other calibration techniques.

Spring constant measurements at multiple positions enable detection and correction for cantilever length irregularities. This study also supports the notion that the effective anchoring point of a cantilever is different from the contact point between the cantilever and its supporting structure. Thus the effective length of a cantilever could be slightly longer than a value measured from the contact point.

While this article is focused on studying AFM cantilevers using an instrumented indenter method, the technique can also be used to measure spring constants of other objects such as MEMS components and colloidal probes. As an example, we have successfully measured the spring constant of a colloidal probe used in adhesion research,¹¹ by orienting the colloid probe upside down on the instrumented indenter stage and pressing directly on the center of the attached microsphere with the indenter tip.

ACKNOWLEDGMENTS

The authors acknowledge Dr. Robert F. Cook for constructive discussions. They also thank Hysitron, Inc., especially Dr. Oden Warren and Lance Kuhn, for their valuable help.

¹A. L. Weisenhorn, P. K. Hansma, T. R. Albrecht, and C. F. Quate, *Appl. Phys. Lett.* **54**, 2651 (1989).

²E. Meyer, H. J. Hug, and R. Bennewitz, *Scanning Probe Microscopy: The Lab on a Tip* (Springer, New York, 2003).

³P. C. Braga and D. Ricci, *Atomic Force Microscopy: Biomedical Methods and Applications* (Humana, Totowa, NJ, 2004).

⁴*Nanoparticles: From Theory to Application*, edited by G. Schmid (Wiley, Weinheim, 2004).

⁵C. A. Clifford and M. P. Seah, *Appl. Surf. Sci.* **252**, 1915 (2005).

⁶*Nanotribology: Critical Assessment and Research Needs*, edited by S. M. Hsu and Z. C. Ying (Kluwer, Boston, 2003).

⁷H. J. Butt, B. Cappella, and M. Kappl, *Surf. Sci. Rep.* **59**, 1 (2005).

⁸B. Cappella and G. Dietler, *Surf. Sci. Rep.* **34**, 1 (1999).

⁹R. Carpick and M. Salmeron, *Chem. Rev. (Washington, D.C.)* **97**, 1163 (1997).

¹⁰E. Meyer, H. Heinzelmann, P. Grütter, T. Jung, H. R. Hidber, H. Rudin, and H. J. Güntherodt, *Thin Solid Films* **181**, 527 (1989).

¹¹J. Grobelny, N. Pradeep, D.-I. Kim, and Z. C. Ying, *Appl. Phys. Lett.* **88**, 091906 (2006).

¹²C. P. Green, H. Lioe, J. P. Cleveland, R. Proksch, P. Mulvaney, and J. E. Sader, *Rev. Sci. Instrum.* **75**, 1988 (2004).

¹³N. A. Burnham, X. Chen, C. S. Hodges, G. A. Matei, E. J. Thoreson, C. J. Roberts, M. C. Davies, and S. J. B. Tendler, *Nanotechnology* **14**, 1 (2003).

¹⁴C. T. Gibson, D. A. Smith, and C. Roberts, *Nanotechnology* **16**, 234 (2005).

¹⁵C. A. Clifford and M. P. Seah, *Nanotechnology* **16**, 1666 (2005).

¹⁶D. Lange, H. Baltes, and O. Brand, *Cantilever-Based CMOS Nano-Electro-Mechanical Systems* (Springer, New York, 2002).

¹⁷C. Liu, *Foundations of MEMS* (Prentice-Hall, Englewood Cliffs, NJ, 2005).

¹⁸J. P. Cleveland, S. Manne, D. Bocek, and P. K. Hansma, *Rev. Sci. Instrum.* **64**, 403 (1993).

¹⁹J. E. Sader, J. W. M. Chon, and P. Mulvaney, *Rev. Sci. Instrum.* **70**, 3967 (1999).

²⁰J. L. Hunter and J. Bechhoefer, *Rev. Sci. Instrum.* **64**, 1868 (1993).

²¹J. E. Sader, *J. Appl. Phys.* **84**, 64 (1998).

²²R. Lévy and M. Maaloum, *Nanotechnology* **13**, 33 (2002).

²³A. W. McFarland and J. S. Colton, *J. Micromech. Microeng.* **15**, 1060 (2005).

²⁴A. Torii, M. Sasaki, K. Hane, and S. Okuma, *Meas. Sci. Technol.* **7**, 179 (1996).

²⁵C. T. Gibson, G. S. Watson, and S. Myhra, *Nanotechnology* **7**, 259 (1996).

²⁶M. Tortonese and M. Kirk, *Proc. SPIE* **3009**, 53 (1997).

²⁷C. Su, L. Huang, and K. Kjoller, *Ultramicroscopy* **100**, 233 (2004).

²⁸G. S. Gates and M. G. Reitsma (unpublished).

²⁹P. J. Cumpson, J. Hedley, and P. Zhdan, *Nanotechnology* **14**, 918 (2003).

³⁰P. J. Cumpson, P. Zhdan, and J. Hedley, *Ultramicroscopy* **100**, 241 (2004).

³¹N. Morel, M. Ramonda, and Ph. Tordjeman, *Appl. Phys. Lett.* **86**, 163103 (2005).

³²M. A. Poggi, A. W. McFarland, J. S. Colton, and L. A. Bottomley, *Anal. Chem.* **77**, 1192 (2005).

³³J. D. Holbery, V. L. Eden, M. Sarikaya, and R. M. Fisher, *Rev. Sci. Instrum.* **71**, 3769 (2000).

³⁴Certain instruments and materials are identified to adequately specify the experimental procedure. Such identification does not imply recommendation or endorsement by the National Institute of Standards and Technology, nor does it imply that the materials or instruments identified are necessarily the best available for the purpose.

³⁵S. P. Timoshenko and J. N. Goodier, *Theory of Elasticity* (McGraw-Hill, New York, 1983).

³⁶R. S. Gates and J. R. Pratt, *Meas. Sci. Technol.* **17**, 2852 (2006).

³⁷Unless otherwise noted in this article, the errors represent statistical uncertainties (1 standard deviation).

³⁸J. R. Pratt, D. T. Smith, D. B. Newell, J. A. Kramar, and E. Whinton, *J. Mater. Res.* **19**, 366 (2004).

³⁹B. D. Jensen, F. Bitsie, and M. P. de Boer, *Proc. SPIE* **3875**, 61 (1999).